

**NOVEL ELECTROSPUN TITANIUM (IV) OXIDE COMPOSITE HOLLOW  
FIBERS AS ANODE IN LITHIUM-ION BATTERIES**

Tanatchporn Sirimekanont

A Thesis Submitted in Partial Fulfilment of the Requirements  
for the Degree of Master of Science  
The Petroleum and Petrochemical College, Chulalongkorn University  
in Academic Partnership with  
The University of Michigan, The University of Oklahoma,  
Case Western Reserve University, and Institut Français du Pétrole  
2013

I28372578

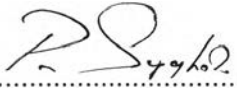
**Thesis Title:** Novel Electrospun Titanium (IV) Oxide Composite  
Hollow Fibers as Anode in Lithium-ion Batteries  
**By:** Tanatchporn Sirirmekanont  
**Program:** Polymer Science  
**Thesis Advisors:** Prof. Pitt Supaphol

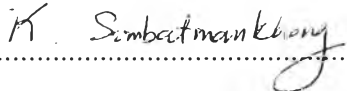
---

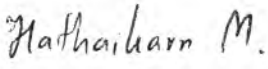
Accepted by The Petroleum and Petrochemical College, Chulalongkorn University, in partial fulfilment of the requirements for the Degree of Master of Science.

  
..... College Dean  
(Asst. Prof. Pomthong Malakul)

**Thesis Committee:**

  
.....  
(Prof. Pitt Supaphol)

  
.....  
(Dr. Korakot Sombatmankhong)

  
.....  
(Asst. Prof. Hathaikarn Manuspiya)

## ABSTRACT

5472049063: Polymer Science Program  
Tanatchporn Sirimekanont: Novel Electrospun Titanium (IV) Oxide  
Composite Hollow Fibers as Anode in Lithium-ion Batteries.  
Thesis Advisors: Prof. Pitt Supaphol and Dr. Korakot  
Sombatmankhong 117 pp.  
Keywords: Electrospinning/ Lithium-ion batteries/ Anode/ Titanium oxide  
nanofibers/ Hollow fibers

Nanostructured transition metal oxides have been developed as electrode materials in Lithium-ion Batteries (LIBS) due to their ability to provide high capacity and improved cycling performance. Among these types, titanium oxide ( $\text{TiO}_2$ ) has attracted considerable interest owing to its high lithium intercalation property, minimal toxicity and small volume change during cycling.  $\text{TiO}_2$ , however, has low ionic and electronic conductivity. Therefore, this present work will focus on the structural modification of  $\text{TiO}_2$  nanofibers to improve their efficiency. Accordingly, the hollow  $\text{ZnO-TiO}_2$  and  $\text{Ag}_2\text{O-TiO}_2$  composite hollow fibers will be prepared through coaxial electrospinning of the colloidal solution consisting of Titanium (IV) isopropoxide/ Poly (vinyl acetate)/ Zn particles and Ag particles in case of  $\text{Ag}_2\text{O-TiO}_2$  fibers, followed by calcination in air at  $500\text{ }^\circ\text{C}$  1 h. Both of added Zn and Ag particles are employed as seeds to generate the growth of ZnO and  $\text{Ag}_2\text{O}$  crystals on the surface of  $\text{TiO}_2$  using the hydrothermal treatment at various times and temperatures. The average diameter of both types of the products obtained after hydrothermal treatment increased with increasing time and temperature of hydrothermal treatment. XRD patterns revealed well crystalline features of anatase  $\text{TiO}_2$  with ZnO, and  $\text{Ag}_2\text{O}$ . Additionally, the surface area of the obtained hollow fibers was observed by BET surface area. Among the hydrothermally treated  $\text{ZnO-TiO}_2$  composite hollow fibers, the fibers which were treated at  $115\text{ }^\circ\text{C}$  0.5 h provided the highest surface area ( $25.164\text{ m}^2\text{g}^{-1}$ ) compared to the other hydrothermally treated ones. But in case of  $\text{Ag}_2\text{O-TiO}_2$  composite hollow fibers, the fibers which were treated at  $110\text{ }^\circ\text{C}$  1 h provided the highest surface area ( $44.960\text{ m}^2\text{g}^{-1}$ ).

## บทคัดย่อ

ธนัชพร ศิริเมฆานนท์ : วัสดุโครงสร้างเส้นใยกลวงเชิงประกอบ ไททาเนียม ออกไซด์ ชนิดใหม่สำหรับการประยุกต์ใช้เป็นขั้วแอโนดในลิเทียมไอออน แบตเตอรี่ (Novel Electrospun Titanium (IV) Oxide Composite Hollow Fibers as Anode in Lithium-ion Batteries) อ. ที่ปรึกษา : ศ. ดร. พิชญ์ สุภผล และ ดร. กรกช สมบัติมั่นคง 117 หน้า

โครงสร้างระดับนาโนของ ทรานซิชั่น เมทัล ออกไซด์ ได้รับการพัฒนาอย่างต่อเนื่อง ในการทำเป็นอิเล็กโทรดในลิเทียมไอออน แบตเตอรี่ โดย ไททาเนียม ออกไซด์ ( $\text{TiO}_2$ ) ได้รับความสนใจอย่างมาก เนื่องจากมีโครงสร้างผลึกที่เหมาะสมในการให้ลิเทียมไอออนแทรกตัวใน ปริมาณสูง, ความเป็นพิษต่ำ, และเกิดการเปลี่ยนแปลงทางปริมาตรน้อยระหว่างกระบวนการให้ และคายประจุ แต่อย่างไรก็ตาม ไททาเนียม ออกไซด์ มีความสามารถในการนำไอออน และอิเล็กตรอนต่ำ ดังนั้นงานวิจัยนี้จึงมุ่งศึกษาวิธีการปรับปรุงลักษณะพื้นผิวเส้นใยไททาเนียม ออกไซด์ เพื่อปรับปรุงประสิทธิภาพการนำไฟฟ้า โดยเส้นใยกลวงซึ่งเป็นวัสดุเชิงประกอบของ ซิงค์ ออกไซด์-ไททาเนียม ออกไซด์ และ ซิลเวอร์ ออกไซด์-ไททาเนียม ออกไซด์ ถูกเตรียมจาก สารละลายคอลลอยด์ของ ไททาเนียม ไอโซโพรพอกไซด์ (TIP)/ พอลิไวนิล อะซิเตท (PVAc)/ อนุภาคของซิงค์ (Zn particles) และ ซิลเวอร์ (Ag particles) ตามลำดับ ผ่านเทคนิค การปั่นเส้นใย ด้วยไฟฟ้าสถิตย์แบบร่วมแกน (coaxial electrospinning) ตามด้วยกระบวนการเผา (calcination) ที่ 500 องศา เป็นเวลา 1 ชั่วโมง โดยอนุภาคของซิงค์ และ ซิลเวอร์ที่เติมลงไป จะถูกใช้เพื่อ เหนี่ยวนำให้เกิดการเติบโตของผลึกซิงค์ ออกไซด์ และ ซิลเวอร์ ออกไซด์ บนผิวของเส้นใยกลวง ผ่านกระบวนการให้ความร้อนด้วยน้ำ (hydrothermal treatment) ที่สภาวะต่างๆ จากผลการทดลอง พบว่าขนาดเส้นใยเฉลี่ยของวัสดุทั้งสองชนิดเพิ่มขึ้นตามเวลาและอุณหภูมิ ภายใต้กระบวนการให้ ความร้อนด้วยน้ำ จากผลเอกซเรย์ดิฟแฟรกชัน (XRD) พบว่าเส้นใยกลวงทั้งสองชนิดประกอบ โครงสร้างผลึกของอะนาทาส ไททาเนียม ออกไซด์ ร่วมกับ ซิงค์ ออกไซด์ และ ซิลเวอร์ ออกไซด์ นอกจากนี้ พื้นที่ผิวของวัสดุโครงสร้างเส้นใยกลวงเชิงประกอบ ไททาเนียม ออกไซด์ทั้งสองชนิด ได้ถูกตรวจสอบโดยเซอร์เฟส แอเรีย อะนาไลเซอร์ (BET) ผลการทดสอบพบว่าวัสดุโครงสร้าง เส้นใยกลวงเชิงประกอบของซิงค์ ออกไซด์- ไททาเนียม ออกไซด์ที่สภาวะ 115 องศา 0.5 ชั่วโมง ให้ค่าพื้นที่ผิวสูงสุด ส่วนวัสดุโครงสร้างเส้นใยกลวงเชิงประกอบของซิลเวอร์ออกไซด์-ไททา นีเนียม ออกไซด์ที่สภาวะ 110 องศา ชั่วโมง ให้ค่าพื้นที่ผิวสูงสุด

## ACKNOWLEDGEMENTS

This work has provided a valuable experience and a lot of knowledge to the author. It would not have been possible without the guidance and the support of several individuals who in one way or another contributed and extended their valuable assistance in the preparation and completion of this study. I would like to express my deepest appreciation to all of them.

First and foremost, I would like to offer my sincerest gratitude to my advisor, Prof. Pitt Supaphol, who continues to support and give excellent guidance and encouragements. Dr. Korakot Sombatmankhong, who acted as my thesis co-advisor, has supplied many necessary things, assistance, and good advices throughout my work. They were always available for my problems I had regarding this work. I would like to extremely thank them for their generous supports, persistent helps and patience that bring me the good opportunity to make this work successful.

Besides my advisor and co-advisor, I would like to specially thank Asst. Prof. Hataikarn Manuspiya for being my advisory committee member and giving me the insightful comments and recommendations.

My sincere thank also goes to all faculties and staffs of the petroleum and petrochemical College for their kind aids to simplify the work.

Also, I would like to express my deep appreciation to Ph.D. students in my group for their suggestions and constant helps as well as their friendliness that made me feel comfortable to be a part of this group. Moreover, special thank goes to all my PPC friends for their kindly helping and encouragements.

This thesis work is funded by the Petroleum and Petrochemical College; and the National Center of Excellence for Petroleum, Petrochemicals, and Advanced Materials, Thailand.

Eventually, the author would like to express the sincerest thankfulness to my family for their limitable supports, priceless encouragement and endless love throughout these two years.

## TABLE OF CONTENTS

	<b>PAGE</b>
Title Page	i
Abstract (in English)	iii
Abstract (in Thai)	iv
Acknowledgements	v
Table of Contents	vi
List of Tables	x
List of Figures	xiii
<b>CHAPTER</b>	
<b>I INTRODUCTION</b>	<b>1</b>
<b>II LITERATURE REVIEW</b>	<b>3</b>
2.1 Lithium-ion Batteries (LIBs)	3
2.2 Materials for Lithium-ion Batteries	4
2.2.1 Cathode Materials	4
2.2.2 Electrolyte Materials	6
2.2.3 Anode Materials	9
2.3 Electrospinning Process	12
2.3.1 Electrospinning Apparatus	14
2.3.2 Modeling of Electrospinning Process	14
2.3.3 Parameters of Electrospinning Process	17
2.3.4 Coaxial Electrospinning	18
2.4 Hydrothermal Synthesis	21
2.5 Crystal Growth and Nucleation	21
2.5.1 Nucleation	22
2.5.2 Crystal Growth	22
2.6 Nanofibrous Materials	23
2.7 The Development of Electrospun Fibrous Anode Materials in Lithium-ion Batteries	26

<b>CHAPTER</b>	<b>PAGE</b>
2.7.1 Lithium Metals	26
2.7.2 The Low Intrinsic Electrical Conductivity of Electrode Materials	27
2.7.3 Transition Metal Oxides	29
2.7.4 Zero-strain Insertion Anode Materials	29
2.7.5 Volume Expansion and Contraction of Anode Materials	30
2.7.6 Si-based Anodes	31
2.7.7 Other Improvements	32
<b>III EXPERIMENTAL</b>	<b>41</b>
3.1 Materials	41
3.1.1 Materials Used for Coaxial Electrospinning	41
3.1.2 Materials Used for Hydrothermal Treatment	41
3.1.3 Materials Used for Electrochemical Characterization	41
3.2 Equipment	41
3.2.1 Scanning Electron Microscope (SEM)	41
3.2.2 Transmission Electron Microscope (TEM)	42
3.2.3 X-ray Diffraction (XRD)	42
3.2.4 Surface Area Analyzer (Autosorp-1MP)	42
3.2.5 Attenuated Total Reflectance-Fourier Transform Infrared Spectrometer (ATR-FTIR)	42
3.2.6 Maccor Battery Test System Series 4000	42
3.3 Methodology	42
3.3.1 The Effect of Operating Voltage to the Morphology of Synthesized Fibers	42
3.3.2 The Effect of Calcination Process to the Crystal Structure of Synthesized Fibers	44
3.3.3 The Effect of Surface Modification by Hydrothermal Treatment to the Morphology, Weight, and the Average	

<b>CHAPTER</b>	<b>PAGE</b>
Diameter of Synthesized ZnO/TiO <sub>2</sub> and Ag <sub>2</sub> O/TiO <sub>2</sub> Composite Hollow Fibers	44
3.4 Characterization	46
3.4.1 Scanning Electron Microscope (SEM)	46
3.4.2 Transmission Electron Microscope (TEM)	46
3.4.3 X-ray Diffraction (XRD)	47
3.4.4 Surface Area Analyzer (Autosorp-1MP)	47
3.4.5 Attenuated Total Reflectance-Fourier Transform Infrared Spectrometer (ATR-FTIR)	47
3.5 Electrochemical Characterization	47
3.5.1 Preparation of Materials Used as Anode	48
3.5.2 Preparation of Materials Used as Cathode	48
<b>IV RESULTS AND DISCUSSION</b>	<b>49</b>
4.1 The Effect of Operating Voltage to the Morphology of Synthesized Fibers	49
4.1.1 TiO <sub>2</sub> Hollow Fibers, Zn/TiO <sub>2</sub> , and Ag/TiO <sub>2</sub> Composite Hollow Fibers	49
4.1.2 TiO <sub>2</sub> Fibers	52
4.2 The Effect of Calcination Process to the Morphology and the Crystal Structure of Synthesized Fibers	53
4.2.1 Calcination Condition at Different Time and Temperature	53
4.3 The Effect of Surface Modification by Hydrothermal Treatment to the Morphology, Weight, and the Average Diameter of Synthesized ZnO/TiO <sub>2</sub> and Ag <sub>2</sub> O/TiO <sub>2</sub> Composite Hollow Fibers	69
4.3.1 Adjusting the Hydrothermal Treatment Condition under the Fixed Time for 1 Hour at Various Temperatures	71



<b>CHAPTER</b>	<b>PAGE</b>
4.3.2 Adjusting the Hydrothermal Treatment Condition under the Fixed Temperature at 115 °C at Various Times	86
4.4 Lithium Ion Battery Study	101
<b>V CONCLUSIONS AND RECOMMENDATIONS</b>	103
5.1 Conclusions	103
5.2 Recommendations	105
<b>REFERENCES</b>	106
<b>APPENDIX</b>	111
<b>Appendix A</b> Experimental Data of BET Surface Area Analysis	111
<b>CURRICULUM VITAE</b>	117

## LIST OF TABLES

<b>TABLE</b>		<b>PAGE</b>
2.1	Advantages and disadvantages of each process for fiber-formation	25
4.1	The average diameter of the pre-calcined TiO <sub>2</sub> hollow fibers	51
4.2	The Percentage of Crystallinity	56
4.3	The details of crystallite size at different conditions	56
4.4	The average diameter (μm) of calcined TiO <sub>2</sub> hollow fibers at different calcinations conditions	61
4.5	Assignments for FT-IR absorption bands for poly(vinyl acetate)	64
4.6	The average diameter of fibers before and after calcination	65
4.7	Cross sectional SEM images and TEM images of calcined TiO <sub>2</sub> hollow fibers, Zn/TiO <sub>2</sub> composite hollow fibers, and Ag/TiO <sub>2</sub> composite hollow fibers	67
4.8	The atomic percentage of calcined composite hollow fibers	69
4.9	The average diameter of ZnO-TiO <sub>2</sub> composite hollow fibers after hydrothermal treatment for 1 h	73
4.10	The weight of ZnO-TiO <sub>2</sub> composite hollow fibers before and after hydrothermal treatment for 1 h	74
4.11	The atomic percentage of hydrothermally treated ZnO-TiO <sub>2</sub> composite hollow fibers for 1 h at various temperatures	75
4.12	The crystallite size of ZnO outgrowths at various temperatures	78
4.13	The average diameter of Ag <sub>2</sub> O-TiO <sub>2</sub> composite hollow fibers after hydrothermal treatment for 1 h	80
4.14	The weight of Ag <sub>2</sub> O-TiO <sub>2</sub> composite hollow fibers before and after hydrothermal treatment for 1 h	81

<b>TABLE</b>	<b>PAGE</b>
4.15 The atomic percentage of hydrothermally treated $\text{Ag}_2\text{O-TiO}_2$ composite hollow fibers for 1 h at different temperatures	83
4.16 The crystallite size of $\text{Ag}_2\text{O}$ outgrowths at various temperatures	85
4.17 The average diameter of $\text{ZnO-TiO}_2$ composite hollow fibers after hydrothermal treatment at $115\text{ }^\circ\text{C}$	88
4.18 The weight of $\text{ZnO-TiO}_2$ composite hollow fibers before and after hydrothermal treatment at $115\text{ }^\circ\text{C}$	89
4.19 The atomic percentage of hydrothermally treated $\text{ZnO-TiO}_2$ composite hollow fibers at $115\text{ }^\circ\text{C}$ at various times	90
4.20 The crystallite size of $\text{ZnO}$ outgrowths at various times	91
4.21 The average diameter of $\text{Ag}_2\text{O-TiO}_2$ composite hollow fibers after hydrothermal treatment for 1 h	94
4.22 The weight of $\text{Ag}_2\text{O-TiO}_2$ composite hollow fibers before and after hydrothermal treatment at $115\text{ }^\circ\text{C}$	95
4.23 The atomic percentage of hydrothermally treated $\text{Ag}_2\text{O-TiO}_2$ composite hollow fibers at $115\text{ }^\circ\text{C}$ at various times	96
4.24 The crystallite size of $\text{Ag}_2\text{O}$ outgrowths at various times	98
4.25 BET surface area of the obtained materials	100
A1 Raw data of multi-point BET of $\text{TiO}_2$ fibers	112
A2 Raw data of multi-point BET of $\text{TiO}_2$ hollow fibers	112
A3 Raw data of multi-point BET of calcined $\text{Zn/TiO}_2$ composite hollow fibers	113
A4 Raw data of multi-point BET of $\text{ZnO-TiO}_2$ composite hollow fibers at $115\text{ }^\circ\text{C}$ 1 h	113
A5 Raw data of multi-point BET of $\text{ZnO-TiO}_2$ composite hollow fibers at $115\text{ }^\circ\text{C}$ 0.75 h	114
A6 Raw data of multi-point BET of $\text{ZnO-TiO}_2$ composite hollow fibers at $115\text{ }^\circ\text{C}$ 0.5 h	114

<b>TABLE</b>		<b>PAGE</b>
A7	Raw data of multi-point BET of calcined Ag/TiO <sub>2</sub> composite hollow fibers	115
A8	Raw data of multi-point BET of Ag <sub>2</sub> O-TiO <sub>2</sub> composite hollow fibers at 110 °C 1 h	115
A9	Raw data of multi-point BET of Ag <sub>2</sub> O-TiO <sub>2</sub> composite hollow fibers at 115 °C 1 h	116
A10	Raw data of multi-point BET of Ag <sub>2</sub> O-TiO <sub>2</sub> composite hollow fibers at 120 °C 1 h	116

## LIST OF FIGURES

FIGURE	PAGE
2.1 Lithium-ion cell operation, during charging lithium ions intercalate into the anode, the reverse occurs during discharge.	4
2.2 Schematic illustration of a typical Li-ion battery: (a) Aluminum current collector; (b) Oxide active material; (c) Porous separator soaked with liquid electrolyte; (d) Inhomogeneous SEI layer; (e) Graphite active material and (f) Copper current collector.	8
2.3 Mechanism of $\text{Li}^+$ ion conduction in intrinsic (dry) SPE.	8
2.4 Three types of carbon.	10
2.5 Schematic representation of an electrospinning apparatus ( $r$ , radius of the capillary; $R$ , curvature radius of the electrode used) and Taylor cones. (a) Formation of Taylor cone in an applied electric field. (b) Taylor cone ejects fluid jet. (c) Surface tension causes cone shape to relax. Jet stream starts out in stable straight region, then becomes unstable, partly owing to charge repulsion, typically showing a whipping or spiraling motion.	12
2.6 Whipping motion occurred in rapid acceleration zone.	13
2.7 A schematic of an electrospinning setup.	14
2.8 Illustrations of (a) A short segment of a garland yarn, (b) Details of the conglutinated solid fibers, and (c) A diagram of a loop in a segment of one fiber and another loop.	17
2.9 The experimental setup of coaxial electrospinning.	19
2.10 High-magnification SEM micrographs and TEM images inserts of C-CNFW carbonized at 850 °C.	19

<b>FIGURE</b>	<b>PAGE</b>
2.11 FE-SEM images of HCNFs carbonized at various carbonization temperatures: (a) 800, (b) 1000, (c) 1200, and (d) 1600 °C.	20
2.12 Schematic representation of processes involved in the crystal growth:(1) Transport of solute to a position nearthe crystal surface; (2) diffusion throughboundary layer; (3) adsorption onto crystalsurface; (4) diffusion over the surface;(4*) desorption from the surface; (5) attachmentto a step or edge; (6) diffusion alongthe step or edge; (7) Incorporation into kinksite or step vacancy.	23
2.13 Artistic representations of (a) Woven fabrics, (b) Nonwoven fabrics (c) nonwoven electrospun mat detail visualizing a soldering-like attachment.	24
2.14 The SEM image for the cross-section of the protection layer.	27
2.15 SEM (1000X) of carbon materials cycled at different discharge rates. (A) Carbon cycled at 1C; (B) carbon cycled at 2C discharge rate; (C) and (D) carbon cycled at 3C discharge rate.	28
2.16 Evolution of the SEI film on the surface of carbon when the battery is continued to be cycled.	28
2.17 Galvanostatic discharge/charge curves for the first cycle.	31
2.18 The SEM image of C/Si = 3.3:1 composite nanofibers cycled for 15 cycles at 0.1 C.	32
2.19 Discharge capacities of the fibers measured at different current densities from 100 to 1000 mAhg <sup>-1</sup> .	33
2.20 Electrochemical tests of C/Li or Fe <sub>3</sub> O <sub>4</sub> /C/Li half cells: discharge capacity versus cycles of the nanofibers.	34
2.21 The TEM images of (a) pristine 1D-TiO <sub>2</sub> , (b) Ag/1D-TiO <sub>2</sub> , and (c) Au/1D-TiO <sub>2</sub> .	35

<b>FIGURE</b>	<b>PAGE</b>
2.22 Cycle performance on the discharge capacities of the test cells at the constant current rate.	35
2.23 The SEM; (A and B) and FE-SEM; (C) images of hydrothermally treated nanofibers.	36
2.24 The galvanostatic charge-discharge curves for the prepared TiO <sub>2</sub> -ZnO nanostructure.	37
2.25 Cycling performance of TiO <sub>2</sub> /PCNFs (PAN:PMMA=2:1, 3:1 and 5:1) and TiO <sub>2</sub> /CNFs (PAN:PMMA=1:0) at different current densities of 25, 50, 100, 200, 400 and 800 mA g <sup>-1</sup> .	38
2.26 The TEM images (a) and (b) of the as-prepared nonwoven TiO <sub>2</sub> and TiO <sub>2</sub> /Ag films after calcination at 500 °C for 1 h in air, respectively.	39
2.27 The Cycling behaviors of the anatase TiO <sub>2</sub> powder, TiO <sub>2</sub> and TiO <sub>2</sub> /Ag hollow fibers.	39
2.28 The FE-SEM images of Si core/C shell nanofibers: (a) low and (b) high magnifications.	40
4.1 SEM images (magnification = 5000X; scale bar = 10.0 μm) of the pre-calcined TiO <sub>2</sub> hollow fibers under the fixed condition of 19 cm working distance at operating voltage of (a) 15 kV, (b) 17 kV, (c) 19 kV, (d) 21 kV, (e) 23 kV, and (f) 25 kV.	50
4.2 The average diameter of pre-calcined TiO <sub>2</sub> hollow fibers as a function of applied voltage (across a fixed working distance of 17 cm).	51
4.3 SEM images (magnification = 5000X; scale bar = 10.0 μm) of (a) pre-calcined Zn/TiO <sub>2</sub> and (b) pre-calcined Ag/TiO <sub>2</sub> composite hollow fibers under the proper electrospinning condition of 15 kV/17 cm.	52

<b>FIGURE</b>	<b>PAGE</b>
4.4 SEM images (magnification = 5000X; scale bar = 10.0 $\mu\text{m}$ ) of the pre-calcined $\text{TiO}_2$ fibers under the proper electrospinning condition of 15 kV/17 cm.	53
4.5 XRD results of $\text{TiO}_2$ hollow fibers before calcination.	54
4.6 XRD results of $\text{TiO}_2$ hollow fibers at various calcination conditions.	55
4.7 SEM images of the calcined $\text{TiO}_2$ hollow fibers (15 kV/17 cm) at different calcination conditions; at (a-1) low and (a-2) high magnifications of 500 $^\circ\text{C}/1\text{h}$ , at (b-1) low and (b-2) high magnifications of 500 $^\circ\text{C}/2\text{h}$ , at (c-1) low and (c-2) high magnifications of 500 $^\circ\text{C}/3\text{h}$ , at (d-1) low and (d-2) high magnifications of 600 $^\circ\text{C}/1\text{h}$ , at (e-1) low and (e-2) high magnifications of 600 $^\circ\text{C}/2\text{h}$ , at (f-1) low and (f-2) high magnifications of 600 $^\circ\text{C}/3\text{h}$ , at (g-1) low and (g-2) high magnifications of 650 $^\circ\text{C}/1\text{h}$ , at (h-1) low and (h-2) high magnifications of 650 $^\circ\text{C}/2\text{h}$ , and at (i-1) low and (i-2) high magnifications of 600 $^\circ\text{C}/3\text{h}$ .	59
4.8 The average diameter of calcined $\text{TiO}_2$ hollow fiber at 500 $^\circ\text{C}$ , 600 $^\circ\text{C}$ , and 650 $^\circ\text{C}$ as a function of calcination time.	60
4.9 The average diameter of calcined $\text{TiO}_2$ hollow fiber at 1 h, 2 h, and 3 h as a function of calcination temperature.	60
4.10 FTIR spectrum of (a) pre-calcined $\text{TiO}_2$ hollow fiber and (b) $\text{TiO}_2$ hollow fiber calcined at 500 $^\circ\text{C}$ 1 h. (The electrospinning condition was 15kV/17cm).	62
4.11 FTIR spectrum of (a) pre-calcined $\text{TiO}_2$ fiber and (b) $\text{TiO}_2$ fiber calcined at 500 $^\circ\text{C}$ 1 h. (The electrospinning condition was 15kV/17cm).	62



<b>FIGURE</b>	<b>PAGE</b>
4.12 FTIR spectrum of (a) pre-calcined Zn/TiO <sub>2</sub> composite hollow fibers and (b) Zn/TiO <sub>2</sub> composite hollow fibers calcined at 500 °C 1 h. (The electrospinning condition was 15kV/17cm).	63
4.13 FTIR spectrum of (a) pre-calcined Ag/TiO <sub>2</sub> composite hollow fibers and (b) Ag/TiO <sub>2</sub> composite hollow fibers calcined at 500 °C 1 h. (The electrospinning condition was 15kV/17cm).	63
4.14 SEM images (magnification = 5000X; scale bar = 10.0 μm) of (a) calcined TiO <sub>2</sub> hollow fibers, (b) calcined Zn/TiO <sub>2</sub> composite hollow fibers, (c) calcined Ag/TiO <sub>2</sub> composite hollow fibers and (d) calcined TiO <sub>2</sub> fibers under the proper calcination condition of 500 °C for 1 h.	65
4.15 SAED patterns of (a) calcined TiO <sub>2</sub> hollow fibers, (b) Zn/TiO <sub>2</sub> composite hollow fibers, and (c) Ag/TiO <sub>2</sub> composite hollow fibers.	68
4.16 EDX results of (a) calcined Zn/TiO <sub>2</sub> composite hollow fibers and (b) Ag/TiO <sub>2</sub> composite hollow fibers.	68
4.17 SEM images (magnification = 15000X; scale bar = 3.00 μm) of hydrothermally treated ZnO-TiO <sub>2</sub> composite hollow fibers for 1 h at (a and b) 110 °C, (c and d) 115 °C, and (e and f) 120 °C.	72
4.18 The average diameter of hydrothermally treated ZnO-TiO <sub>2</sub> composite hollow fibers for 1 h at various temperatures.	73
4.19 The obtained weight of ZnO outgrowths for 1 h at different temperatures.	74
4.20 EDX results of hydrothermally treated ZnO-TiO <sub>2</sub> composite hollow fibers for 1 h at (a) 110 °C, (b) 115 °C, and (c) 120 °C.	75

<b>FIGURE</b>	<b>PAGE</b>
4.21 XRD patterns of (a) Zn/TiO <sub>2</sub> composite hollow fibersobtained after calcination and ZnO-TiO <sub>2</sub> composite hollow fibersobtained after hydrothermal treatment for 1 h at (b) 110 °C, (c) 115 °C, and (d) 120 °C.	77
4.22 SAED patterns of ZnO-TiO <sub>2</sub> composite hollow fibersobtained after hydrothermal treatment for 1 h at (a) 110 °C, (b) 115 °C, and (c) 120 °C.	77
4.23 SEM images of hydrothermally treated Ag <sub>2</sub> O-TiO <sub>2</sub> composite hollow fibersfor 1 h at (a) 110 °C, (c) 115 °C, and (e) 120 °C at magnification = 15000X; scale bar = 3.00 μm and at (b) 110 °C, (d) 115 °C, and (f) 120 °C at magnification = 35000X; scale bar = 1.00 μm.	79
4.24 The average diameter of hydrothermally treated Ag <sub>2</sub> O-TiO <sub>2</sub> composite hollow fibersfor 1 h at various temperatures.	80
4.25 The obtained weight of Ag <sub>2</sub> O outgrowths for 1 h at various temperatures.	81
4.26 EDX results of hydrothermally treated Ag <sub>2</sub> O-TiO <sub>2</sub> composite hollow fibersfor 1 h at (a) 110 °C, (b) 115 °C, and (c) 120 °C.	82
4.27 XRD patterns of (a) Ag/TiO <sub>2</sub> composite hollow fiberswhich acquired after calcination and Ag <sub>2</sub> O-TiO <sub>2</sub> composite hollow fibers obtained after hydrothermal treatment for 1 h at (b) 110 °C, (c) 115 °C, and (d) 120 °C.	84
4.28 SAED patterns of Ag <sub>2</sub> O-TiO <sub>2</sub> composite hollow fibersacquired after hydrothermal treatment for 1 h at (a) 110 °C, (b) 115 °C, and (c) 120 °C.	85
4.29 SEM images(magnification = 15000X; scale bar = 3.00 μm) of hydrothermally treated ZnO-TiO <sub>2</sub> composite hollow fibersat 115 °C for (a and b) 0.5 h, (c and d) 0.75 h, and (e and f) 1 h.	86

<b>FIGURE</b>	<b>PAGE</b>
4.30 The average diameter of hydrothermally treated ZnO-TiO <sub>2</sub> composite hollow fibers at 115 °C as a function of time.	87
4.31 The obtained weight of ZnO outgrowths at 115 °C at different times.	88
4.32 EDX results of hydrothermally treated ZnO-TiO <sub>2</sub> composite hollow fibers at 115 °C for (a) 0.5 h, (b) 0.75 h, and (c) 1 h.	89
4.33 XRD patterns of (a) Zn/TiO <sub>2</sub> composite hollow fibers obtained after calcination and ZnO-TiO <sub>2</sub> composite hollow fibers obtained after hydrothermal treatment at 115 °C for (b) 0.5 h, (c) 0.75 h, and (d) 1 h.	91
4.34 SEM images of hydrothermally treated Ag <sub>2</sub> O-TiO <sub>2</sub> composite hollow fibers at 115 °C for (a) 0.5 h, (c) 0.75 h, and (e) 1 h at magnification = 15000X; scale bar = 3.00 μm and for (b) 0.5 h, (d) 0.75 h, and (f) 1 h at magnification = 35000X; scale bar = 1.00 μm.	92
4.35 The average diameter of hydrothermally treated Ag <sub>2</sub> O-TiO <sub>2</sub> composite hollow fibers at 115 °C as a function of time.	92
4.36 The obtained weight of Ag <sub>2</sub> O outgrowths at 115 °C as a function of time.	94
4.37 EDX results of hydrothermally treated Ag <sub>2</sub> O-TiO <sub>2</sub> composite hollow fibers at 115 °C for (a) 0.5 h, (b) 0.75 h, and (c) 1 h.	95
4.38 XRD patterns of (a) Ag/TiO <sub>2</sub> composite hollow fibers acquired after calcination and Ag <sub>2</sub> O-TiO <sub>2</sub> composite hollow fibers obtained after hydrothermal treatment at 115 °C for (b) 0.5 h, (c) 0.75 h, and (d) 1 h.	97
4.39 The digital photos of the prepared (a) anode, (b) cathode, and (c) separator.	101
4.40 Charge curve of hydrothermally treated ZnO-TiO <sub>2</sub> composite hollow fibers under the condition of 115 °C 0.5 h.	102